Tunable 2D electron gas at the $LaAlO_3/SrTiO_3(001)$ interface

I. V. Maznichenko,[1,*] S. Ostanin,[1] A. Ernst,[2,3] and I. Mertig[1,3]
[1]*Institute of Physics, Martin Luther University Halle-Wittenberg, D-06099 Halle, Germany*
[2]*Institute of Theoretical Physics, Johannes Kepler University, A-4040 Linz, Austria*
[3]*Max Planck Institute of Microstructure Physics, Weinberg 2, D-06120 Halle, Germany*

(Received 27 March 2019; published 22 July 2019)

Currently, the formation of a two-dimensional electron gas (2DEG) at the TiO_2/LaO-terminated interface between $LaAlO_3$ (LAO) grown on $SrTiO_3$(001) (STO) is well understood. The role of the polarity of LAO and its critical thickness for the formation of 2DEG have been established. Here, we show how 2DEG can be tuned externally by changing electronic balance at the LAO(001) surface or, alternatively, at the intrinsically hole-doped AlO_2/SrO interface of LAO/STO heterostructures. The effects of liquid gating at LAO(001) and imperfected AlO_2/SrO were simulated in the framework of the first-principles Green function method within the coherent-potential approximation. We evaluated the Fermi surface cross sections, which were computed varying the degree of chemical disorder. These findings may be extremely important for potential application of 2DEG.

DOI: 10.1103/PhysRevMaterials.3.074006

I. INTRODUCTION

The two-dimensional electron gas (2DEG), which can appear at the interface between robustly insulating perovskites, such as epitaxial $LaAlO_3$ (LAO) grown on the $SrTiO_3$ (001) (STO) substrate, is completely established nowadays [1–5]. This 2DEG can be easily detected with side electrodes or by tunneling measurements between the electron gas and metallic electrodes on LAO [6]. Regarding the LAO/STO interface, any explanation of its 2DEG invokes the arguments of the so-called polar discontinuity [7–10] related to the LAO (001) side, which represents alternately charged planes $[LaO]^+$ and $[AlO_2]^-$. At the TiO_2/LaO-terminated LAO/STO interface, therefore, each interfacial La transfers half of an electron into the neighboring and formally neutral TiO_2 layer that decreases the oxidation state of interfacial Ti. The 2DEG scenario based to the $Ti^{3.5+}$ valence state was successfully modeled from first principles [11]. Apart from LAO/STO, there is a family of composite perovskites for which the TiO_2/LaO termination is formed unavoidably. In particular, 2DEG appears between STO (001) and $LaFeO_3$ (LFO) [12]. Li *et al.* [13] reported that the crystalline and partially amorphous ABO_3/STO (A=La, Pr, Nd and B=Al, Ga) interfaces become conducting for ABO_3 thicker than four unit cells (u.c.).

All epitaxially grown perovskite heterostructures contain intrinsic oxygen vacancies and substitutional cations near the interfaces [14,15]. Interfacial defects may induce additional charged carriers. Oxygen vacancy, for instance, enhances there the n-type doping [16], whereas the La/Sr interfacial mixing [17] may suppress 2DEG. Experimentally, after oxygen annealing (when the O redox mechanism is removed), the LAO/STO interfaces prepared at 500 °C and below become insulating, while samples prepared at 515 °C and above are conducting [13].

The *ab initio* calculations [18] suggest that strong reconstruction may compensate the dipolar electric field in LAO overlayers and, therefore, sustain the insulating behavior up to 5 u.c. LAO. The most recent and systematic *ab initio* calculations of LAO/STO [19] in which the cation intermixing across the interface and oxygen vacancies were modeled, within the Green function method, have suggested that the 2DEG effect starting from the defect-free interfacial composition may be enhanced by the presence of oxygen vacancies and substituted cations.

So far, only a very limited number of experiments have been performed to study how the 2DEG of a buried interface can be tuned externally. Since perovskites grow in complete unit cells on the atomically clean and TiO_2-terminated STO (001) substrate [20], the LAO (001) surface is AlO_2 terminated. There are two options to change the electronic balance of this AlO_2 termination: either by capping layers or by liquid gating at the surface. Liquid gating, in particular, allows one to reversibly change the amount of oxygen vacancies [21–23]. The widely used example of capping is the LAO/STO heterostructure [24]. Concerning intrinsically imperfect LAO layers, the vacancy-filling effect could be controlled there by the degree of crystallinity by varying the growth temperatures. However, the capped system excludes practically the scenario of switchable 2DEG, whereas the utilization of liquid gating at the LAO surface may do that.

Over the past decade, electrolyte gating has become a powerful technique for accumulating large carrier densities at the surfaces of oxides [25,26]. Regarding their interfaces, such as LAO/STO, it was shown that extremely high mobility of 2DEG up to $\sim 10^4$ $cm^2/(V\,s)$ can be realized by the ionic liquid-assisted field effect [27]. This mobility is one order of magnitude higher than that of silicon-based transistors. Moreover, with the change of the gate voltage and gate

*igor.maznichenko@physik.uni-halle.de

polarity, the controlled depletion of negatively/positively charged carriers can be obtained that, in principle, allows one to vary the 2DEG conductivity from its enhanced value down to zero. The corresponding mechanism can be understood using the terminology of oxygen migration. By choosing the proper gate geometry and polarity, some of the intrinsic O vacancies in LAO and those accommodated at the buried interface can be filled. On the other hand, by switching the gate polarity, the O^{2-} ions can be partially pulled out from the LAO side that makes the composition of LAO and, probably, its buried LAO/STO interface oxygen deficient. Although the switching is not completely reproducible, this allows one to explore the effect of electrolytic gating on the 2DEG of LAO/STO through the measurements of electrical transport, x-ray absorption spectroscopy, and photoluminescence spectra [27–32]. Meanwhile, the controllable formation of 2DEG via ionic liquid gating has been shown recently for the $LaFeO_3$/STO interface [12].

In this work, we investigate from first principles the LAO/STO and its 2DEG, focusing on the long-range disorder at (i) the *p*-type AlO_2/SrO interface and (ii) the LAO surface. In the literature, this issue remains unclear. In all calculations, the LAO film thickness was modeled above critical. First, we modeled the LAO capping, within a supercell approach, keeping the defects at the *p*-type interface and inspecting the 2DEG changes at the *n*-type interface. Here, the use of the coherent-potential approximation (CPA) offers an elegant way to describe oxygen vacancies and cation substitutes in the frameworks of the self-consistent Green function formalism [33]. This approach adequately describes the LAO/STO interfaces [19].

For the scenario of switchable 2DEG at the LAO/STO interface, we used the slab geometry with the AlO_2-terminated LAO (001). Thus, we disclose the electronic conditions at the surface needed to vary the buried 2DEG. The surface electronic balance, which mimics the effect of liquid gating, was simulated here within the CPA.

II. DETAILS OF *AB INITIO* CALCULATIONS

Chronologically, the structural model for the first-principles calculations of LAO/STO was transformed from the initially used superlattice [34,35] to the slab geometry with a vacuum layer [11,16,36–41]. The use of the slab geometry allows one to reproduce 2DEG at the TiO_2/LaO interface. Although the *n* interface remains conducting below the LAO critical thickness of 4 u.c., the use of a superlattice is a good starting point for any reliable *ab initio* calculation [19]. In fact, the use of a superlattice removes the most serious question concerning the electrostatic boundary conditions of free surfaces and their impact on 2DEG.

Here, we calculated the TiO_2/LaO and AlO_2/SrO terminations of LAO/STO simultaneously, within the supercells, which thickness was optimized previously [19]. Thus, we simply combined the 12-u.c.-thick STO and 12-u.c.-thick LAO. The in-plane lattice parameter was fixed to the experimental value of bulk STO ($a_0 = 3.905$ Å) to simulate the epitaxial growth of LAO on the STO substrate. The presence of oxygen vacancies as well as the cation vacancies and substitutes were modeled at the *p*-type AlO_2/SrO interface. This scenario assumes the corresponding changes of 2DEG at the TiO_2/LaO interface. All calculations of perfect and imperfect superlattices were performed using a first-principles Green function method [42,43] based on the multiple-scattering theory within the density functional theory in a generalized gradient approximation (GGA) to the exchange-correlation potential [44]. We used a full charge density treatment to take into account the possible nonsphericity of the crystal potential and the charge density [45]. In this approximation, the charge density and the effective crystal potential are expanded within the Wigner-Seitz (Voronoi) cell into spherical harmonic functions, while the single-scattering *t* matrix is calculated only with the spherical part of the effective potential. Such approach provides a very good precision comparable with a full-potential method [46]. The results of the electronic structure calculations are not sensitive to a particular choice of the Wigner-Seitz (or Voronoi) division of the elementary unit cell. The maximal angular momentum for the Green function and the charge density expansion was taken to be $l_{\max} = 3$ and $L_{\max} = 6$, respectively. The integrals over the Brillouin zone were performed using the $16 \times 16 \times 2$ *k*-point mesh.

The cation intermixing, oxygen, and cation vacancies were simulated using a coherent-potential approximation (CPA) as it implemented within the multiple-scattering theory [33,47]. In this mean-field approach, impurities or other lattice imperfections are described by an effective medium Green function, which is determined in a self-consistent way by embedding single-impurity matrices into the effective medium. Since the CPA is designed for substitutional alloys, atomic relaxations around a defect cannot be taken into account. Therefore, we optimized crystalline structures only for defect-free surfaces and heterostructures tracing by this mainly the chemical impact of disorder. Vacancies were simulated by empty Wigner-Seitz cells of the same geometry as for the host atoms. Oxygen vacancies were also distributed over the O sites near the *p* interface, in the interfacial SrO and AlO_2 layers.

For the second scenario of buried and tunable 2DEG, we used the slab with vacuum. The supercell combines 12 u.c. of STO and 8 u.c. of LAO along [001]. There is the TiO_2/LaO terminated interface only. We modeled the presence of oxygen vacancies as well as excessive oxygens at the AlO_2-terminated LAO (001). This crudely mimics the effect of liquid gating, although the latter should involve dynamically all layers of the LAO side. In this context, we realize that our simplified model differs from the corresponding experimental conditions. Here we study this issue using first principles.

III. 2DEG IN THE LAO/STO HETEROSTRUCTURES: THE EFFECT OF DEFECTIVE *p* INTERFACE

The presence of interfacial defects, such as oxygen and cation vacancies, may crucially change the 2DEG of LAO/STO. This was discussed previously [19] for the case when vacancies are accommodated at the same *n*-type interface where 2DEG appears. Now, we compute 2DEG and its changes by simulating oxygen vacancies at the *p*-type interface. In the right panel of Fig. 1, we plot the conduction/valence band (CB/VB) profile along [001] calculated for the LAO/STO heterostructure, which contains 10% O vacancies in the interfacial $AlO_{1.9}$ layer. The O vacancies

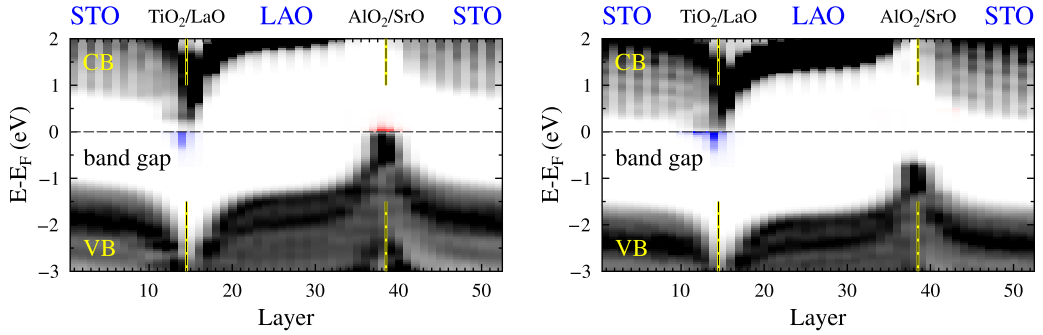

FIG. 1. The conduction/valence band (CB/VB) profiles along [001] in the LAO/STO heterostructure, calculated for the ideal (left panel) and for the 10% O-deficient p interface (right panel). White: the band gap with no density of states.

there should suppress the 2D hole gas (2DHG), which appears in the perfect heterostructure, as shown in the left panel of Fig. 1. We anticipate that for the O-vacancy compositions >10%, the 2DHG disappears completely in this heterostructure, whereas slightly enhanced 2DEG is there. Interestingly, the top valence-band position, which is seen in Fig. 1 and which appears below the Fermi level, corresponds to the $AlO_{2-\delta}$ interfacial layer with $\delta = 0.1$.

To evaluate the changes in 2DEG, we calculated its n-type carrier density which emerges at the Fermi level for different δ. The result is plotted in Fig. 2 as a function of the degree of interfacial oxidation at the p-type interface. With increasing the O-vacancy concentration between $0 < \delta < 0.1$ in both $AlO_{2-\delta}$ and $SrO_{1-\delta}$ interfacial layers, the 2DEG density increases. However, in the case of $SrO_{1-\delta}$, the effect is more pronounced. For instance, the 2DEG density, which emerges mainly in the interfacial and perfect TiO_2 layer, increases from 0.8×10^{13} cm^2 calculated for $\delta = 0$ to 1.8×10^{13} cm^2 and 3.2×10^{13} cm^2 calculated for $AlO_{1.9}$ and $SrO_{0.9}$, respectively. In general, the calculated 2DEG density is in good agreement with the measured values. The explanation of enhanced 2DEG for $\delta > 0$ is obvious. This is because the Fermi level goes up, cutting, therefore, the larger portion from the bottom of the conduction band at the n-type interface.

Additionally, we simulated the effect of the cation-deficient interfacial layers $Al_{1-x}O_2$ and $Sr_{1-x}O$ at the p interface of the LAO/STO heterostructure. This can also be considered as excessive oxygen composition. Obviously, the Al and Sr vacancies accommodated at the p-type interface should enhance the 2DHG there. This is because the Fermi level is shifted down. The band bending near the CB bottom also occurs, which affects the 2DEG density at the opposite n-type interface. In the case of Sr vacancies, our calculations demonstrate that 2DEG remains stable with no changes in its density until the composition $Sr_{0.8}O$, as shown in Fig. 2. It should be noted that the ideal SrO layer was formally neutral and, therefore, to obtain the increase in the 2DEG density due to $Sr_{1-x}O$, an unrealistically large value of $x > 0.3$ is needed. In the case of $Al_{1-x}O_2$, we anticipate that with increasing x up to 10%, the 2DEG density reaches about 1.6×10^{13} cm^2, which is compatible to that simulated with oxygen vacancies in the same interfacial layer. We also modeled the effect of cations intermixing at the p interface of the LAO/STO heterostructure. However, the calculated CB/VB profiles do not show any significant changes since the Fermi level position in the system remains stable.

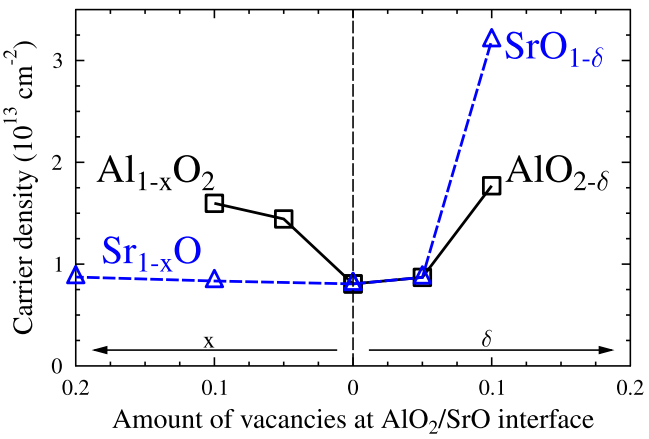

FIG. 2. 2DEG density emerged in the LAO/STO heterostructure vs the degree of interfacial oxidation at the p-type interface.

IV. EFFECT OF THE LAO(001) SURFACE

A. 2DEG beneath chemically perfect surface

The CB/VB profiles, calculated along [001] for the 8-u.c.-thick LAO (001) on 12-u.c.-thick STO, are shown in Fig. 3. We assumed that the crystal structure is cubic, the LAO surface is AlO_2 terminated, and the TiO_2/LaO interface is perfect. To plot the band gap shown in Fig. 3, we used the DOS calculated within each TiO_2 and AlO_2 layers only. Our calculation clearly shows (i) the 2DEG which emerges at the TiO_2/LaO interface and (ii) the weakly p-doped LAO surface. Most importantly, the 2DEG density is 3.2×10^{13} cm^2, which is four times as much as the 2DEG density of the ideal heterostructure. The 2DEG density was integrated over a few interfacial layers along [001]. In Fig. 4, we plot the layer-resolved contributions calculated near the n-type interface for the slab with ideal surface of LAO and for the heterostructure with chemically perfect interfaces. This figure shows how 2DEG enhances in the case of an open surface. In the heterostructure, the LAO thickness was 8 u.c., while its 2DEG density differs insignificantly from that of 12 u.c. thick.

The topmost AlO_2 layer of LAO(001) is not flat. The O positions are always above the Al position. This issue related to the perovskite (001) surface was discussed experimentally and

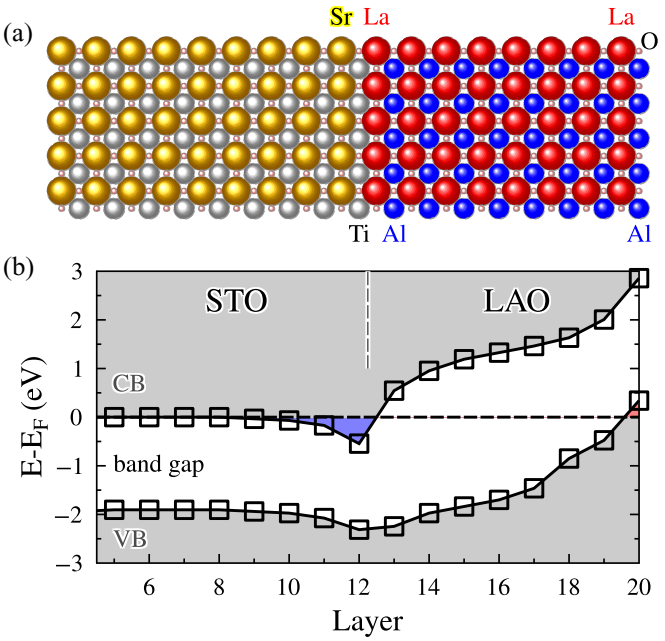

FIG. 3. (a) Atomic structure and (b) the CB/VB profiles along [001] of 8-u.c.-thick LAO (001) grown on 12-u.c.-thick STO. In (a), red balls: La atoms; blue: Al atoms; golden: Sr atoms; gray: Ti atoms; small rose-colored balls: oxygens.

theoretically [20,48]. Here, we relaxed the atomic positions of the topmost layer and, then, the 2DEG density was calculated. The result, which is shown in Fig. 5, indicates that the 2DEG density increases by 0.2×10^{13} cm^2 compared to that of the unrelaxed surface. In addition, we varied the O displacements from the surface AlO_2 layer between -0.08 Å and 0.12 Å. As Fig. 5 shows, the 2DEG density gradually increases when the O-Al separation increases within the topmost layer.

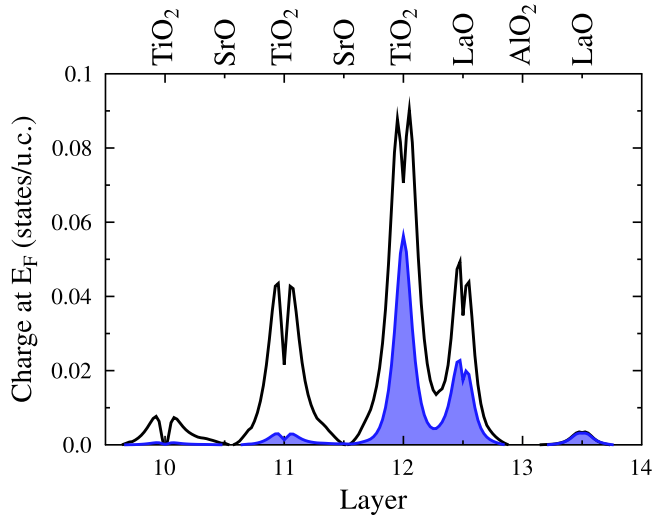

FIG. 4. The layer-resolved contributions to 2DEG calculated along [001] for the perfect LAO/STO heterostructure (filled blue) and chemically perfect LAO/STO (001) surface (black solid line). The same LAO thickness of 8 u.c. was used for the two cases. Atomic layers are labeled and numerated along [001].

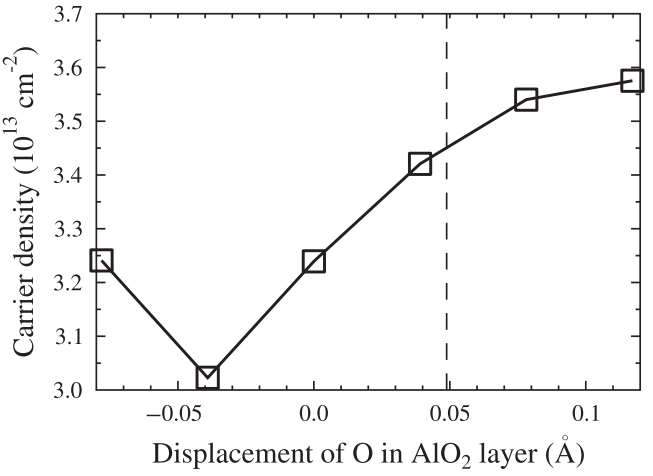

FIG. 5. 2DEG density emerged in LAO/STO (001) and calculated as a function of the O-Al displacement within the surface AlO_2 layer. The vertical dashed line corresponds to the O positions after relaxation.

B. Effect of oxygen doping at the LAO surface

We simulated both the O vacancies and excessive oxygen compositions at the surface. This means that the oxygen adatom sits above the topmost Al atom. This result, which crudely mimics the effect of liquid gating, is plotted in Fig. 6. In the case of an oxygen-deficient surface, $AlO_{2-\delta}$, with increasing $0 < \delta < 0.1$, the 2DEG density increases up to 3.6×10^{13} cm^2. For $0.1 < \delta < 0.2$, the calculated density of 2DEG remains robust at about 3.5×10^{13} cm^2. For the O-rich LAO surface, $AlO_{2+\delta}$, the calculated 2DEG density increases gradually with increasing δ, as shown in Fig. 6. One can see that this effect of doped surface is similar to that which is seen in Fig. 2 for the LAO/STO heterostructure. The effect of enhanced 2DEG, which was calculated for the surface composition $AlO_{2+\delta}$, can be understood in terms of dipole interactions between the *p*-charged surface and *n*-charged interface through the insulating barrier. With increasing hole carriers at the surface, the band bending results in extra

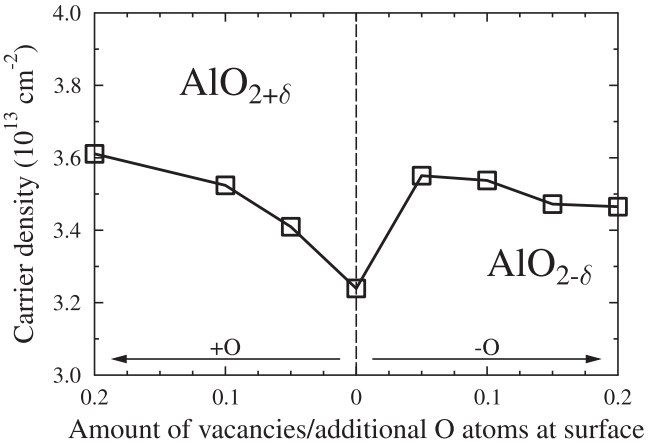

FIG. 6. 2DEG density emerged at the *n*-type LAO/STO (001) interface and plotted as a function of the degree of oxidation of the surface $AlO_{2-\delta}$ layer.

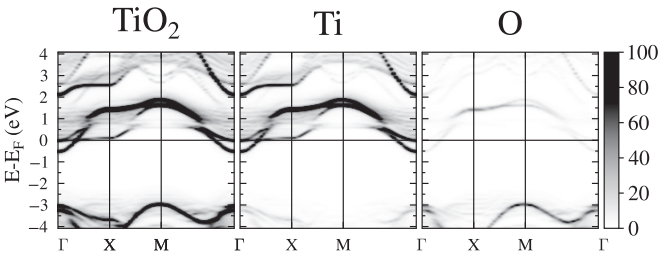

FIG. 7. Bloch spectral function of LAO/STO (001), which is projected on interfacial Ti and plotted along the high-symmetry directions of the 2D Brillouin zone.

interfacial electrons to keep the charge balance. It should be noted that the case of $AlO_{2+\delta}$ seems artificial. This composition is not favorable energetically. The relaxed oxide surface always tends to charge neutrality. In this context, the O-deficient surface composition $AlO_{2-\delta}$ represents a more robust scenario of enhanced 2DEG.

C. Transport-related properties of 2DEG

To show the key features of the electronic states of LAO/STO (001), we plot in Fig. 7 the Bloch spectral function, projected on the interfacial TiO_2 layer and its Ti and O sites. These projections are plotted along the high-symmetry directions of the 2D Brillouin zone. One can see there how the Ti d conduction band crosses E_F around $k = (0, 0)$, while the O contribution is the result of hybridization.

In the case of heterostructure, the conduction Ti d band, which crosses E_F of LAO/STO and which forms the 2DEG there, is isotropic. One can see that in the top panels of Fig. 8 as a plotted spherical Fermi contour. In fact, we show in Fig. 8 the (001) cross sections of the Bloch spectral function projected on each atomic layer near the n-type interface. The middle panels of Fig. 8 correspond to the ideal surface composition AlO_2, while the bottom panels display the projections calculated for the surface layer $AlO_{1.9}$, which contains the O vacancies.

For the free surface, the 2D picture of its conducting Fermi contours is much more complicated, as compared to the corresponding heterostructure. First, the spherical Fermi contour, which is formed by the Ti d states from the interfacial TiO_2 layer, dominates around the Γ point. Although the LaO interfacial layer contributes there insignificantly, this is the result of hybridization. Second, a rhombic Fermi spot appears at Γ due to the d states of interfacial Ti and another one from the second TiO_2 layer. Besides, there are rather narrow Fermi arms along the directions [10], which come from the two TiO_2 layers and which make a whole Fermi picture weakly anisotropic. The doped LAO surface yields extra Fermi contours. This is shown, for instance, in the bottom panels of Fig. 8 for the surface composition $AlO_{1.9}$. The valuable Fermi contributions are the ellipses centered at Γ and elongated along ΓX. These contours are formed by the Ti d states from the second and interfacial layers of STO. Therefore, the anisotropy of conductivity may enhance when the charge balance at the surface differs from its nominal AlO_2.

Thus, the presence of a free surface makes the 2DEG spatially extended, which is also seen in Fig. 4. As a result, the two new Fermi cross sections (a spot and arms), which additionally appear at the spherical contour, may bring a variety to the electron effective mass associated with the 2DEG. When the surface layer contains oxygen vacancies, the Fermi-contour picture becomes even more sophisticated and anisotropic since 2DEG becomes spatially extended. This is shown in the bottom panels of Fig. 8. We anticipate, therefore, that the electron effective mass can range between 0.4 and

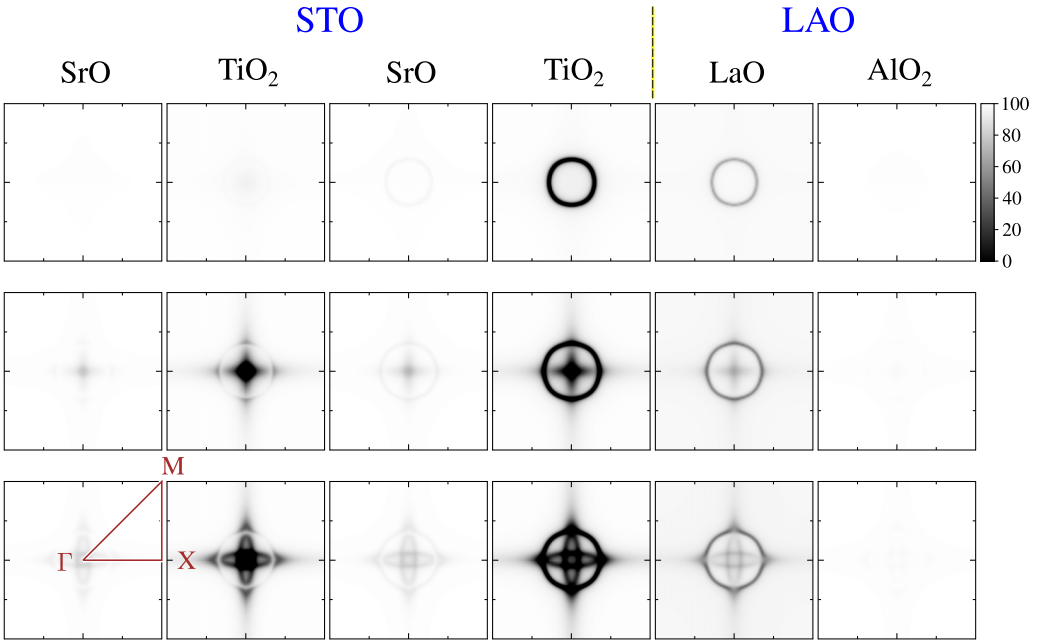

FIG. 8. The (001) cross sections of the Bloch spectral function projected on several atomic layers near the n-type interface of LAO/STO. The top and middle panels correspond to the perfect heterostructure and perfect surface layer AlO_2, respectively. The bottom panels shows the result calculated for the surface composition $AlO_{1.9}$.

0.6 m_e, which is in good agreement with the reported values measured so far [40,49,50].

V. SUMMARY

Using *ab initio* calculations, we simulated the enhancement of 2DEG at the TiO_2/LaO-terminated interface of LAO/STO (001), which may occur when the degree of oxidation changes at the LAO surface. This model mimics the effect of liquid gating, which has been observed in LAO/STO above the critical thickness of LAO. The degree of doping below and above the AlO_2 surface composition was modeled, within the Green function method and the coherent potential approximation. Based on our findings, we conclude that in the case of an ideal surface of LAO, the 2DEG density that emerged at the buried interface is much more pronounced, as compared to the defect-free LAO/STO heterostructure. Moreover, we anticipate that the 2DEG density can be enhanced and controlled by the presence of both extra oxygens or oxygen vacancies at the AlO_2-terminated surface.

By inspecting the calculated Fermi cross sections, which appear in LAO/STO (001) due to 2DEG, we conclude that the LAO surface could affect the transport-related properties of the studied system. As a result, the two additional and weakly anisotropic transport channels are added to the highly isotropic spherical Fermi contour that enhances the electron effective mass within its wider range between 0.4 and 0.6 m_e. We believe that our findings can stimulate further experimental and theoretical studies of the effect of liquid gating in LAO/STO and similar interfaces of polar discontinuity.

ACKNOWLEDGMENT

This work was supported by *Sonderforschungsbereich* SFB 762, "Functionality of Oxide Interfaces."

[1] S. Stemmer and S. J. Allen, Annu. Rev. Mater. Res. **44**, 151 (2014).
[2] A. Ohtomo and H. Y. Hwang, Nature (London) **427**, 423 (2004).
[3] S. Thiel, G. Hammerl, A. Schmehl, C. W. Schneider, and J. Mannhart, Science **313**, 1942 (2006).
[4] N. Nakagawa, H. Y. Hwang, and D. A. Muller, Nat. Mater. **5**, 204 (2006).
[5] H. Y. Hwang, Y. Iwasa, M. Kawasaki, B. Keimer, N. Nagaosa, and Y. Tokura, Nat. Mater. **11**, 103 (2012).
[6] G. Singh-Bhalla, C. Bell, J. Ravichandran, W. Siemons, Y. Hikita, S. Salahuddin, A. F. Hebard, H. Y. Hwang, and R. Ramesh, Nat. Phys. **7**, 80 (2010).
[7] J. Goniakowski, F. Finocchi, and C. Noguera, Rep. Prog. Phys. **71**, 016501 (2008).
[8] C. Noguera and J. Goniakowski, Chem. Rev. **113**, 4073 (2013).
[9] N. C. Bristowe, P. Ghosez, P. B. Littlewood, and E. Artacho, J. Phys.: Condens. Matter **26**, 143201 (2014).
[10] C. Noguera and J. Goniakowski, *Oxide Materials at the Two-Dimensional Limit*, Springer Series in Materials Science Vol. 234 (Springer International Publishing, Switzerland, 2016), p. 201.
[11] R. Pentcheva and W. E. Pickett, J. Phys.: Condens. Matter **22**, 043001 (2010).
[12] P. Xu, W. Han, P. M. Rice, J. Jeong, M. G. Samant, K. Mohseni, H. L. Meyerheim, S. Ostanin, I. V. Maznichenko, I. Mertig *et al.*, Adv. Mater. **29**, 1604447 (2017).
[13] C. Li, Z. Liu, W. Lü, X. R. Wang, A. Annadi, Z. Huang, S. Zeng, Ariando, and T. Venkatesan, Sci. Rep. **5**, 13314 (2015).
[14] L. Qiao, T. C. Droubay, V. Shutthanandan, Z. Zhu, P. V. Sushko, and S. A. Chambers, J. Phys.: Condens. Matter **22**, 312201 (2010).
[15] L. Qiao, T. Droubay, T. Kaspar, P. Sushko, and S. Chambers, Surf. Sci. **605**, 1381 (2011).
[16] N. Pavlenko, T. Kopp, E. Y. Tsymbal, J. Mannhart, and G. A. Sawatzky, Phys. Rev. B **86**, 064431 (2012).
[17] V. Vonk, J. Huijben, D. Kukuruznyak, A. Stierle, H. Hilgenkamp, A. Brinkman, and S. Harkema, Phys. Rev. B **85**, 045401 (2012).
[18] R. Pentcheva and W. E. Pickett, Phys. Rev. Lett. **102**, 107602 (2009).
[19] I. Maznichenko, S. Ostanin, V. Dugaev, I. Mertig, and A. Ernst, Phys. Rev. Mater. **2**, 074003 (2018).
[20] H. L. Meyerheim, F. Klimenta, A. Ernst, K. Mohseni, S. Ostanin, M. Fechner, S. Parihar, I. V. Maznichenko, I. Mertig, and J. Kirschner, Phys. Rev. Lett. **106**, 087203 (2011).
[21] J. Jeong, N. Aetukuri, T. Graf, T. D. Schladt, M. G. Samant, and S. S. Parkin, Science **339**, 1402 (2013).
[22] J. Jeong, N. B. Aetukuri, D. Passarello, S. D. Conradson, M. G. Samant, and S. S. Parkin, Proc. Natl. Acad. Sci. **112**, 1013 (2015).
[23] S. G. Altendorf, J. Jeong, D. Passarello, N. B. Aetukuri, M. G. Samant, and S. S. Parkin, Adv. Mater. **28**, 5284 (2016).
[24] A. K. Singh, T.-C. Wu, M.-C. Chen, M.-Y. Song, W.-L. Lee, C.-P. Su, and M.-W. Chu, Phys. Rev. Mater. **2**, 114009 (2018).
[25] J. Ye, S. Inoue, K. Kobayashi, Y. Kasahara, H. Yuan, H. Shimotani, and Y. Iwasa, Nat. Mater. **9**, 125 (2010).
[26] M. Li, T. Graf, T. D. Schladt, X. Jiang, and S. S. P. Parkin, Phys. Rev. Lett. **109**, 196803 (2012).
[27] S. Zeng, W. Lü, Z. Huang, Z. Liu, K. Han, K. Gopinadhan, C. Li, R. Guo, W. Zhou, H. H. Ma *et al.*, ACS Nano **10**, 4532 (2016).
[28] S. W. Zeng, X. M. Yin, T. S. Herng, K. Han, Z. Huang, L. C. Zhang, C. J. Li, W. X. Zhou, D. Y. Wan, P. Yang, J. Ding, A. T. S. Wee, J. M. D. Coey, T. Venkatesan, A. Rusydi, and A. Ariando, Phys. Rev. Lett. **121**, 146802 (2018).
[29] E. Maniv, Y. Dagan, and M. Goldstein, MRS Adv. **2**, 1243 (2017).
[30] I. Pallecchi, F. Telesio, D. Li, A. Fête, S. Gariglio, J.-M. Triscone, A. Filippetti, P. Delugas, V. Fiorentini, and D. Marré, Nat. Commun. **6**, 6678 (2015).
[31] P. Gallagher, M. Lee, T. A. Petach, S. W. Stanwyck, J. R. Williams, K. Watanabe, T. Taniguchi, and D. Goldhaber-Gordon, Nat. Commun. **6**, 6437 (2015).
[32] W. Liu, S. Gariglio, A. Fête, D. Li, M. Boselli, D. Stornaiuolo, and J.-M. Triscone, APL Mater. **3**, 062805 (2015).

[33] B. L. Gyorffy, Phys. Rev. B **5**, 2382 (1972).
[34] M. S. Park, S. H. Rhim, and A. J. Freeman, Phys. Rev. B **74**, 205416 (2006).
[35] K. Janicka, J. P. Velev, and E. Y. Tsymbal, Phys. Rev. Lett. **102**, 106803 (2009).
[36] P. R. Willmott, S. A. Pauli, R. Herger, C. M. Schlepütz, D. Martoccia, B. D. Patterson, B. Delley, R. Clarke, D. Kumah, C. Cionca *et al.*, Phys. Rev. Lett. **99**, 155502 (2007).
[37] M. Breitschaft, V. Tinkl, N. Pavlenko, S. Paetel, C. Richter, J. R. Kirtley, Y. C. Liao, G. Hammerl, V. Eyert, T. Kopp *et al.*, Phys. Rev. B **81**, 153414 (2010).
[38] L. Yu and A. Zunger, Nat. Commun. **5**, 5118 (2014).
[39] M. A. Islam, D. Saldana-Greco, Z. Gu, F. Wang, E. Breckenfeld, Q. Lei, R. Xu, C. J. Hawley, X. X. Xi, L. W. Martin *et al.*, Nano Lett. **16**, 681 (2016).
[40] H. Guo, W. A. Saidi, and J. Zhao, Phys. Chem. Chem. Phys. **18**, 28474 (2016).
[41] H. L. Zhuang, L. Zhang, H. Xu, P. Kent, P. Ganesh, and V. R. Cooper, Sci. Rep. **6**, 25452 (2016).
[42] M. Lüders, A. Ernst, M. Däne, Z. Szotek, A. Svane, D. Ködderitzsch, W. Hergert, B. L. Györffy, and W. M. Temmerman, Phys. Rev. B **71**, 205109 (2005).
[43] M. Geilhufe, S. Achilles, M. A. Köbis, M. Arnold, I. Mertig, M. Hergert, and A. Ernst, J. Phys.: Condens. Matter **27**, 435202 (2015).
[44] J. P. Perdew, K. Burke, and M. Ernzerhof, Phys. Rev. Lett. **77**, 3865 (1996).
[45] L. Vitos, J. Kollár, and H. L. Skriver, Phys. Rev. B **55**, 13521 (1997).
[46] M. Asato, A. Settels, T. Hoshino, T. Asada, S. Blügel, R. Zeller, and P. H. Dederichs, Phys. Rev. B **60**, 5202 (1999).
[47] P. Soven, Phys. Rev. **156**, 809 (1967).
[48] M. Fechner, S. Ostanin, and I. Mertig, Phys. Rev. B **77**, 094112 (2008).
[49] Z. Zhong, A. Tóth, and K. Held, Phys. Rev. B **87**, 161102(R) (2013).
[50] A. McCollam, S. Wenderich, M. Kruize, V. Guduru, H. Molegraaf, M. Huijben, G. Koster, D. Blank, G. Rijnders, A. Brinkman *et al.*, APL Mater. **2**, 022102 (2014).